

ARTICLE

DOI: 10.1038/s42004-018-0046-7

OPEN

Gas phase electrochemical analysis of amino acids and their fragments

Maria Calleja¹, Atif Elahi¹ & Daren J. Caruana¹

All chemical reactions involve electron rearrangement within or between molecules. The changes are best studied by methods such as electrochemistry, but these have been developed mainly for liquids and solids rather than gases. This exclusion limits our understanding of electron transfer processes that are central in plasma systems, which are of high scientific, industrial, and environmental importance. Here we describe electrochemical measurements in the gas phase of small organic molecules contained in flame plasma, by probing the redox activity of the resulting chemical fragments using cyclic voltammetry. Unique current-voltage spectra are recorded for eight amino acids and their fragments, through specific electron transfer reactions at the solid/gas interface. We identify and assign Faradaic peaks in the current-voltage spectra to the fragments using stable analogues of the fragments and in situ mass spectroscopy. We show that this approach provides unambiguous identification of organic based molecules, with a sensitivity and power of speciation to rival mass spectrometry.

¹Christopher Ingold Laboratory, Department of Chemistry, University College London, 20 Gordon Street, London WC1H 0AJ, UK. Correspondence and requests for materials should be addressed to D.J.C. (email: D.J.Caruana@ucl.ac.uk)

Electron transfer between atoms or molecules brings about the remarkable wealth of chemistry that underpins all fundamental processes, ranging from star formation to sustaining life^{1,2}. Electron exchange is also essential in industry and research to achieve desired chemical transformations. Consequently, techniques that yield an improved understanding of redox reactions are highly important. Electrochemical analysis is conventionally performed at the solid/liquid interface to investigate electron attachment reactions at an electrode surface under mutually matching energy levels³. However, the solid/liquid interface imposes a double constraint: analytes outside the solvent's endogenous electrochemical activity range are excluded from detection and the liquid imposes a significant diffusive barrier. The most radical way to overcome these limitations is to completely omit solvent^{4–8}. An important requirement remains, however, to achieve electrical conductivity to sustain charge transfer^{6,9–11}.

Here we present a departure from conventional electrochemistry and measure—in the gas phase—the direct electrochemical reduction of organic compounds via voltammetry. The principle of the approach is schematically summarized in Fig. 1. A target molecule is added to a hydrogen/oxygen flame that serves as gas-phase electrolyte. The flame also fragments the molecule into stable units as well as several transient radical species¹². The latter interact with the working electrode surface by accepting an electron, giving rise to a series of corresponding reduction peaks in the voltammogram. Interference from ions of the hydrogen/oxygen flame is minimal because the target molecule is introduced at approximately $1.2 \pm 0.2 \times 10^{18}$ particles m^{-3} , which is about a thousandfold higher than the background ionisation. The recorded potentials of reduction are defined against a specially developed high temperature reference electrode based on oxygen conducting zirconium oxide (YSZR)¹³. All potentials herein quoted versus this reference.

Results

Gas-phase electrochemical analysis of simple acids and alcohols. To validate the new approach, we first added to the plasma two simple organic species bearing carboxylic acid groups, and recorded the reduction signals. Our working hypothesis was that the functional group would give rise to a radical species, which is measured as a characteristic signature in the voltammograms. Indeed, both methanoic and ethanoic acids yielded a prominent peak at -5.80 ± 0.3 V (Fig. 2a), which most likely represents the

electrochemical reduction of the carboxylate fragment COOH (or HCOO) as indicated by the fragment in the mass spectra (MS) for formic and ethanoic at $45 m/z$, Fig. 2b^{14–16}. In support of the interpretation, amino acid alanine had the same peak. The COOH (or HCOO) fragment as opposed to CO_2 is plausible given the slightly reducing plasma with a high proportion of hydrogen in the premixed flame. Indeed, addition of CO_2 to the flame up to a concentration of 10%/vol gave no measurable reduction signals, most likely due to the corresponding large positive electron attachment energies¹⁷.

In further analysis, ethanoic acid but not methanoic acid displayed an additional peak at -9.0 ± 0.2 V (Fig. 2a). The signal is most likely due to the methyl-derived CH_2^+ fragment, which is seen in supporting MS of ethanoic acids as a peak at $14 m/z$ but not for methanoic acid (Fig. 2b). MS sampling was conducted at the same point where the electrode would be positioned for electrochemical measurements. In support, alanine also showed the peaks in both analysis methods. The high potential of -9.0 ± 0.2 V underscores the advantage of the new gas-phase voltammetry because classical liquid-based electrochemistry with a limited to the range of -2 to $+3$ V vs. NHE due to the breakdown of the solvent, electrode or electrolyte would have not enabled detection.

After establishing that carboxylic acid groups provide unique electrochemical signatures, hydroxyl groups were tested. The voltammograms for methanol and ethanol gave rise to a broad peak at -4.1 ± 0.4 V (Fig. 2a), thereby confirming that the flame-induced fragmentation also yields a unique signature for C–OH. The electrochemical signals stems, however, likely from the oxidized CHO group, which is also detected in MS as $29 m/z$ peak (Fig. 2b). Oxidative fragmentation of alcohols during combustion is well known^{18,19}, (see Supplementary Note 1) and dominates the slightly reducing environment of the plasma. The other electrochemical signal at -8.0 ± 0.3 V of only ethanol possibly reflects a dicarbon fragment not observed in the MS.

Analysis of amino acids. Next, serine was examined to test whether the hydroxyl and the carboxyl group that were previously separately detected can also be identified within one molecule. Indeed, voltammograms of serine displayed a common signature at -4.1 ± 0.4 V similar to the two simple reference alcohols (Fig. 2a). In agreement, negative control alanine lacking the hydroxyl group did not have this signal. In further support, serine

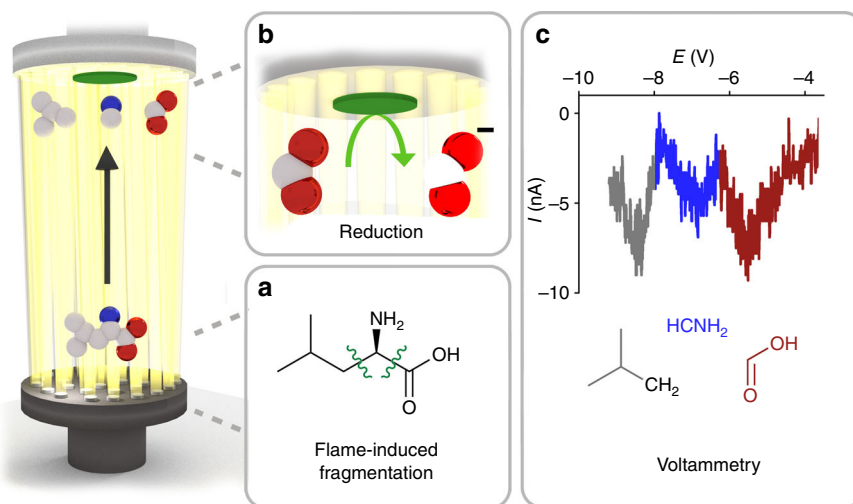


Fig. 1 Schematic of electrochemical analysis of organic species in flame plasma. Showing the flame introduction of organic species followed by **a** fragmentation and **b** electrochemical analysis. The peaks in the voltammetry shown in **c** are assigned the fragments from incomplete combustion

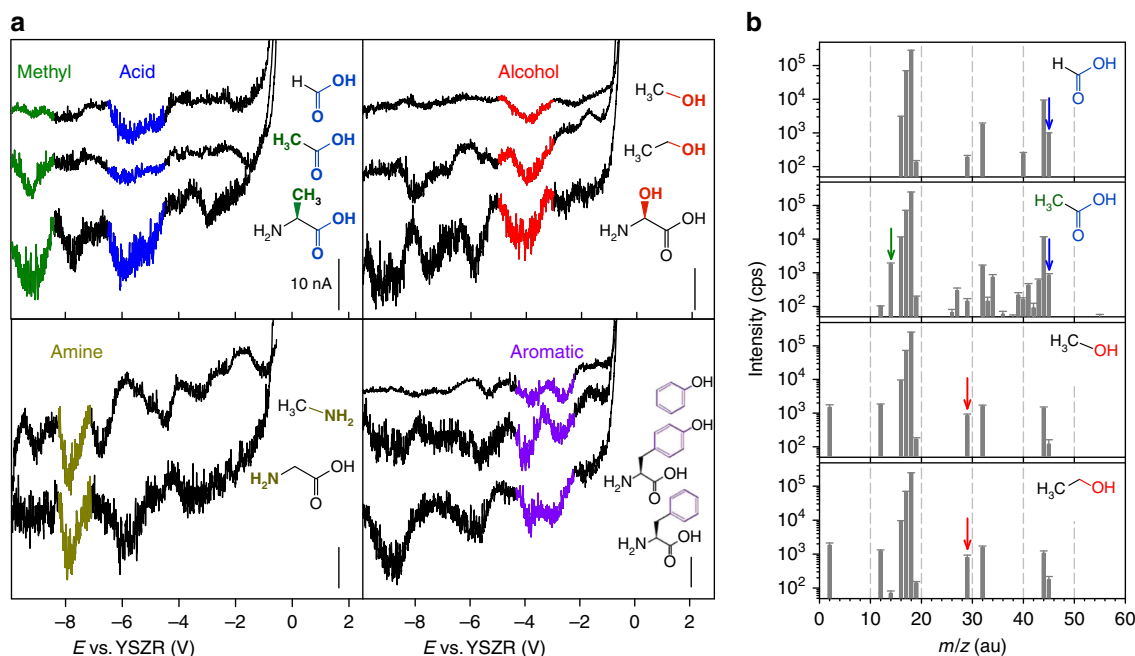


Fig. 2 Voltammetry and in situ MS in flame plasma containing simple organic compounds. **a** Voltammograms of flame containing of methanoic acid, ethanoic acid and alanine, methanol, ethanol and serine, methylamine and glycine, phenol, tyrosine and phenylalanine, introduced into the flame by atomised aqueous solutions of 5 mM, except for tyrosine which was 1 mM. **b** The mass spectra of the flame containing methanoic acid, ethanoic acid, methanol and ethanol, all corrected for the background flame containing deionised water. Coloured arrows indicate masses of interest

featured the acid peak at -5.9 ± 0.15 V, almost identical to the value of methanoic and ethanoic acid at -5.80 ± 0.3 V. Strikingly, both serine and alanine displayed a peak at -7.9 ± 0.2 V, likely reflecting the amine group. This interpretation is supported by a -7.9 ± 0.2 V signal with the same asymmetry for the chemically simpler methylamine but also glycine (Fig. 2a). Methylamine shows other peaks as expected from its known more complex combustion^{20,21}.

Aromatic groups such as phenol and the amino acids tyrosine and phenylalanine similarly gave unique voltammogram peaks. For example, phenol clearly showed two peaks at -3.9 ± 0.3 V and -2.5 ± 0.3 V at approximately the same potentials as for phenylalanine and tyrosine (Fig. 2a). The signals can be associated with the aromatic side groups' ring opening and subsequent breakdown. The peak-to-peak separation, ΔE for phenol and phenylalanine are 1.05 ± 0.10 V and 1.10 ± 0.08 V, respectively, but 0.93 ± 0.08 V for tyrosine, are almost identical. Any subtle differences between them may be due to the different substitution of the benzene ring.

To confirm that gas-phase electrochemistry can distinguish between a range of closely related analyte molecules with different functional groups, a wide set of eight amino acids were examined. The features in the voltammograms for each amino acid, Fig. 3, echo the signatures of the key functional groups of the amino acids, as established from the simple previously analysed molecules (Fig. 2a). For example, the voltammograms of glycine, alanine and serine with peaks at approx. -4.1 , -5.8 , -7.7 and -9.0 V were assigned to the previously established chemical groups of alcohol, acid, amine and methyl groups, respectively. The interpretation is supported by MS as the pattern of fragmentation reflected the electrochemical signals of the three amino acids (Fig. 3). Similarly, the aromatic amino acids gave peaks expected for the loss of the acid group at -5.8 V \pm 0.3 V, and the other features are likely from the breakdown of the aromatic portion. As expected, isomeric amino acids leucine and isoleucine have the same pattern

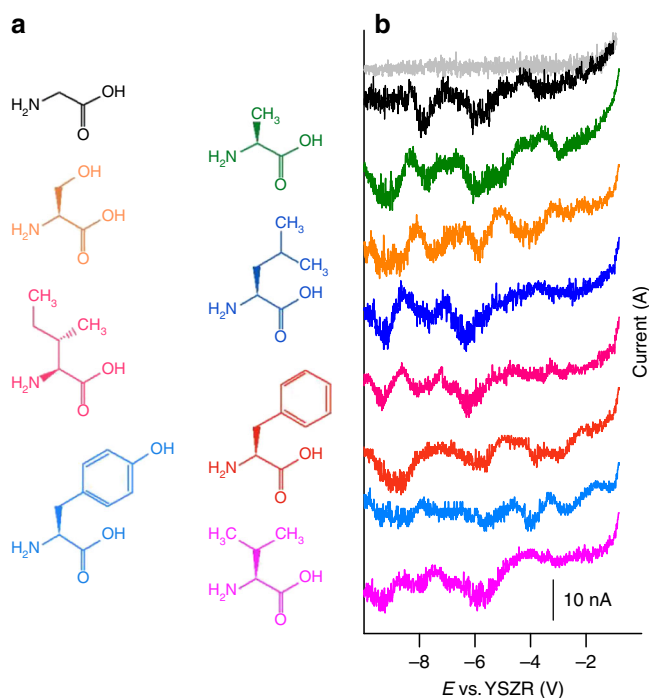


Fig. 3 Voltammetry of the eight amino acids added to the flame plasma. Showing the colour coded chemical structures **a** and the corresponding voltammograms **b** in a flame containing glycine, alanine, serine, leucine, isoleucine, phenylalanine, tyrosine, introduced into the flame by atomised aqueous solutions of 5 mM, except for tyrosine which was 1 mM

(Fig. 3b) with -5.8 , -7.5 and -9.0 V due to decarboxylation, amine, and aliphatic fragments, respectively. The voltammograms valine, leucine and isoleucine differ only in the number or structure of carbons, and hence have related electrochemical

signals as well as patterns of fragmentation as shown by MS in Supplementary Fig. 1.

Mechanistic study. The voltammetry data imply that electrochemical reduction takes place at the electrode surface. To provide direct evidence for this surface-located reaction, in situ Raman spectroscopy was applied, Fig. 4. Therefore, a graphitic electrode was exposed to a flame doped with water containing 5 mM leucine, and Raman spectra were recorded at 1 V steps between 0 V and -10 V and reverse. The analysis focused on Raman carbon G band at 1560 cm^{-1} because it corresponds to the E_{2g} optical mode, where stretching of all bonds with sp^2 atoms is sensitive to redox processes^{22,23}. As shown in Fig. 4b, the band's intensity varies with applied static potential, and strongly correlates with the electrochemical peaks in terms of voltage-dependence and signal strength. This means that at potentials with strong electrochemical reduction, the G band has low intensity. The correlation is the same when the potential is scanned in both directions; it does not occur in the absence of lysine (Fig. 4a). The Raman data hence provides compelling evidence of redox chemistry at the electrode surface in contact with a gaseous plasma.

Theoretical framework. After demonstrating the experimental validity of our electrochemical approach, we next sought to place it within a theoretical framework. Our considerations first focused on the fact that the gas-phase voltammograms feature peaks rather than the step-wise current levels that are typical for liquid-phase electrochemistry (Fig. 5). To account for the peaks, we use the electrode's Fermi energy for electron transfer, E_F , and the characteristic reduction potential, E_R , for the oxidized organic fragments in the gas phase²⁴. Electron transfer between electrode and fragments is assumed to only take place when E_F and E_R energetically overlap (Fig. 5, $E_{F,2} = E_R$). This can be achieved by varying E_F with the potential. By contrast, mismatching energy levels $E_{F,1} < E_R$ or $E_{F,3} > E_R$ do not lead to transfer (Fig. 5). This

explanation is clearly different to the traditional liquid-phase electrochemistry where electron transfer takes place provided the Fermi level is higher than E_R (Fig. 5), as underpinned by the step-wise current levels in traditional voltammograms²⁵.

The uniqueness of gas-phase electrochemistry is underscored by demonstrating that the peaks in the voltammograms represent solely reduction but not oxidation of the molecular fragments. Visually, the absence of oxidation can be inferred from the missing peaks in the positive direction on the voltammogram. The expectation, for a system such as this with efficient hydrodynamic mass transport of oxidised species to the electrode surface, would appear in the voltammogram as a plateau, represented as a blue solid line in Fig. 5. This unique property can also be formalized by Eq. (1), which predicts the current shown as the red solid line in Fig. 5, similar to what we observe experimentally, via integrals for reduction and for oxidation

$$I = nFA \left[m_O C_O \nu_R \int_{-\infty}^{\infty} P_O(E) N_E(E) dE \right] - \left(m_R C_R \nu_O \int_{-\infty}^{\infty} P_R(E) N_E(E) dE \right) \quad (1)$$

where n , F and A , are the number of electrons involved in the reduction, Faraday's constant and electrode area, respectively. The mass transport coefficient to the electrode and the concentration for oxidized (subscript O) and reduced (subscript R) species are represented by m and C respectively, and ν is the frequency for an electron transfer reaction. The integral quantifies the overlap of electron states in the electrode $N(E)$, and the distribution of states in the gas, $P(E)$ as a function of applied potential (see Supplementary Note 2). Using Eq. (1), the calculated I/V traces for and oxidation and reduction process in the gas phase, is shown by the dashed red line in Fig. 5. The absence of oxidation can be molecularly explained by considering the relative magnitudes of m_O and m_R . As both account for molecular transport across the diffusion layer at the electrode surface, term m_O —which is synonymous for supply of oxidised

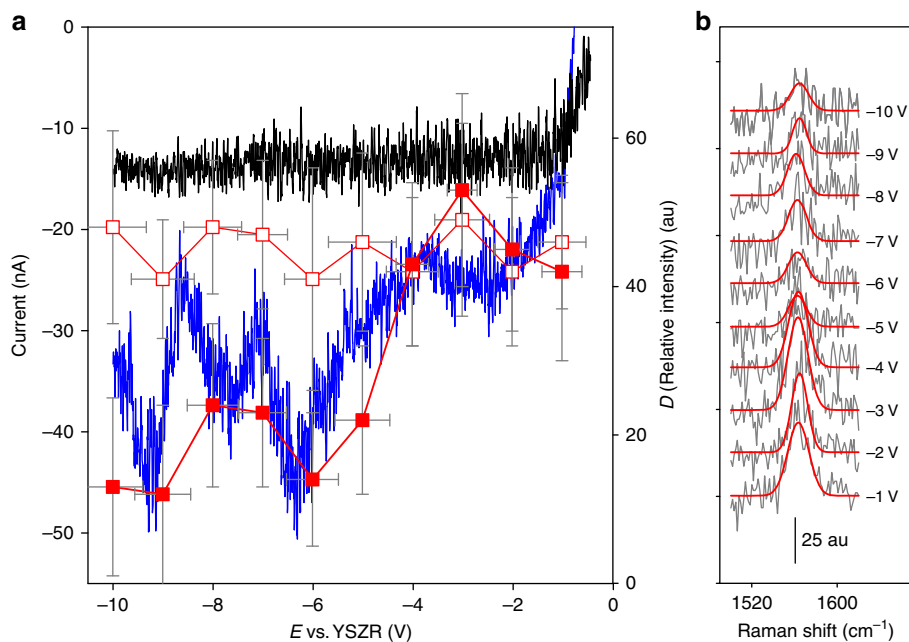


Fig. 4 In situ Raman spectroscopy of the electrode surface under electrochemical control. **a** Voltammogram and potentiodynamic Raman peak height at 1560 cm^{-1} , of a graphite working electrode held at constant potential for 1 minute, in flame plasma doped with pure water (voltammogram, light blue line, potentiodynamic, open squares) and 5 mM leucine (voltammogram, solid blue line; potentiodynamic, solid squares). Error bars indicate the standard error of three measurements. **b** The Raman spectra between 1500 and 1630 cm^{-1} (grey lines) which are fitted to a Gaussian function (red lines), held at potentials from -1 to -10 V vs. YSZR

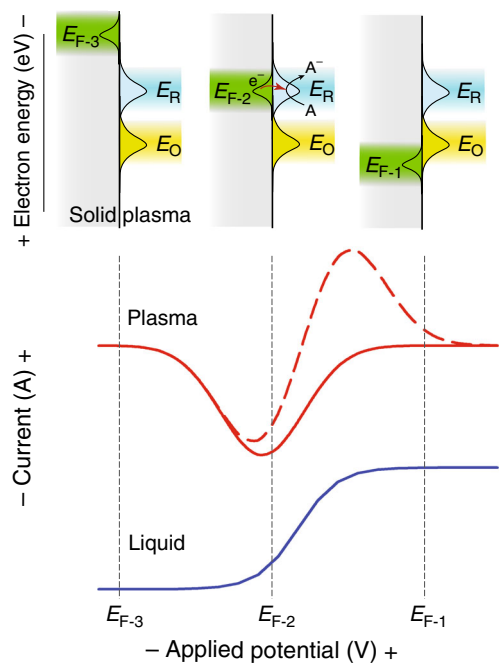


Fig. 5 Schematic diagram relating applied electrochemical potential with electron energy levels and the I/V traces expected. Energy level diagram showing the relationship between electron energy levels expressed as available states at three electrochemical potentials, E_{F-1} , E_{F-2} and E_{F-3} and the gas phase states for the reduced, E_R and oxidized, E_O species. The red traces are the calculated I/V traces using Eq. (1), dashed line is when $m_R = m_O$ and $C_R = C_O$ and solid line when $m_R = 0$ and $C_R = 0$. The blue I/V trace is the equivalent process in liquid electrolytes

species to facilitate reduction—will be high as the uncharged radical fragments can diffuse to the negatively charged electrode surface. By contrast, m_R —equivalent for oxidation—will be vanishingly small because the reduced and hence negatively charged fragment will be electrostatically repelled by the negatively polarized electrode surface. The extent of repulsion can be calculated. A singly charged species will experience an electric field of ca. $50,000 \text{ V m}^{-1}$ when a potential difference of 5 V is applied across a plasma sheath. This will result in an acceleration of $2 \times 10^{11} \text{ m s}^{-2}$ away from the electrode surface.

Discussion

We present a method capable of differentiating a variety of different organic species, which is achieved by adopting a gaseous plasma medium interrogated by electrochemistry. Using a combination of mass spectrometry and doping with a small selection of carefully chosen species, we have successfully assigned the electrochemical signals to the fragmentation products of eight different amino acids. We deduced that certain organic groups give rise to radical species in the flame, which can be reduced electrochemically resolved in applied potential. We present new insights into electrochemical electron attachment in a plasma and present true gas phase electrochemistry of organic species.

This radical departure from conventional liquid phase electrochemistry enables electron attachment events to be measured in the gas phase, which are normally restricted to techniques such as electron beam or photoelectron spectroscopy¹⁷. Perhaps expectedly, there are significant departures from the analogous electron transfer processes in condensed phases. These departures present fruitful theoretical avenues for research to develop a quantum mechanical level understanding of electron transfer

reactions at the solid/gas interface. Whilst we only show measurements between 0 and -10 V here, we expect that there will be a rich electrochemical information to be accessed beyond this range.

The frugal design of the electrode assembly is both robust and simple, presents a very powerful tool for chemical analysis²⁶. We anticipate that this approach extends the utility Langmuir probes by providing chemical information rather than simple conductivity measurements for the development of new plasma diagnostic tools^{27,28}, stimulating new analysers for atomic absorption and inductively coupled plasma.

Methods

Burner design. A specially designed Méker type burner (based on the design described by Goodings and Hayhurst²⁹) used for this study is described in Supplementary Note 3, and Supplementary Figure 2 providing a two-compartment laminar flow flame consisting of a premixed combination of hydrogen, oxygen and nitrogen. Aqueous solutions were prepared using deionised water (Millipore Milli-Q[®] gradient, $<0.05 \text{ S cm}^{-2}$). The solution was introduced into the gas stream in the form of an aerosol created from a modified ultrasonic atomiser (Index Ltd. UK). The burner brass top-plate was cleaned by skimming the top surface, and the holes were carefully cleaned using a 0.5 mm diameter drill before each set of experiments. The burner was mounted vertically on an earthed aluminium table. The dual flames were each served by an independent stream of gases at flow rates of 1.6 , 0.4 and 1.0 L min^{-1} for nitrogen (99.99%), oxygen (99.9+%) and hydrogen (99.995%) (gases supplied by BOC), respectively; with a total flow rate for the entire flame of 6.0 L min^{-1} , shown in Supplementary Note 3. Individually controlled digital mass flow controllers (5850 S, Brooks, USA, with IGI control interface, UK) were used to regulate the flow rates of hydrogen, oxygen and nitrogen. Before reaching the burner, each of the two gas streams were thoroughly mixed in a chamber, which included a blow-out panel to protect against flash back; NB. Premixed hydrogen and oxygen gases are explosive and adequate safety precautions were taken. The gas lines for both streams were identical except for an aerosolization chamber which was used to introduce the organic species to the flame, in the nitrogen line, before the mixing chamber feeding the right-hand section of the flame. In all experiments solution was added to the right-hand flame, the left-hand flame was kept as a clean flame and was used as the reference electrode compartment. The calibration for the delivery of dopants to the right-hand flame is outlined in Supplementary Note 4.

Instrumentation. Electrode surface temperatures, whilst immersed in the flame, were measured using a Thermal Imaging Pyrometer (800–3000 K) model M9100 supplied by Mikron instrument Company Inc. (USA), calibrated to a traceable standard. Cyclic voltammograms were recorded using a potentiostat (Autolab PGSTAT 100, Eco Chemie B.V. supplied by Windsor Scientific Ltd., UK) with 100 V compliance voltage, only the first sweep is presented of the cyclic voltammogram and are referred to as ‘voltammogram’.

Mass spectrometry measurements were carried out using a HPR-60 MBMS (Hiden, UK) an instrument specifically for atmospheric plasma analysis. The Raman measurements were performed using a inVia Raman microscope (Renishaw, UK) with an optic fibre probe, which was focused on the working electrode surface (see Supplementary Figure 3).

Electrode assembly and procedure. Reference electrodes were constructed by thoroughly grinding yttria-stabilised zirconia with a small amount of ethanol to form a homogeneous paste, which was packed into the end of a recrystallized alumina tube (od 2.75 mm , id 1.6 mm , Dynamic Ceramic, UK) to a depth of 3.0 mm , making contact with a tungsten wire (1 mm diameter, Goodfellow, UK) for electrical connection. The counter electrode and working electrode assembly was positioned at 10.0 mm above the burner top. The cylindrical stainless-steel enclosure had a 25.0 mm diameter platinum disc, 2.0 mm thickness held in place at the base of the enclosure. The platinum disc had a 3.0 mm diameter hole at its centre which accommodated the working electrode (see Supplementary Note 3). The entire assembly was positioned over the flame with the hole accommodating the working electrode precisely in the path of the right-hand section of the flame. A gold or pyrolytic graphite rod (Goodfellow Ltd., UK) 2.4 mm diameter served as a working electrode, which was clamped in a ceramic holder (Macor[®]) and precisely positioned in a 3.0 mm hole in a platinum foil counter electrode. Once in the flame, the working electrode surface temperature was $1236 \pm 15 \text{ K}$. The voltammograms were recorded after the electrodes were positioned in the flame for 30 seconds , scanning between 0 to -10 V at a rate of 1 V s^{-1} , which is the optimal scan rate for this media as reported in Ref.¹¹. Three consecutive scans were recorded; the second scan is presented. A fresh reference electrode was used for every series of voltammogram. Error on the potentials quoted are calculated based on the movement of the stability of the peak upon repetitive cycling, minimum number of cycles is 6.

Data availability. All data generated during the current study are available from the corresponding author on reasonable request.

Received: 19 April 2018 Accepted: 17 July 2018

Published online: 23 August 2018

References

1. Rumbach, P., Bartels, D. M., Sankaran, R. M. & Go, D. B. The solvation of electrons by an atmospheric-pressure plasma. *Nat. Commun.* **6**, 7248 (2015).
2. Caruana, D. J. & Holt, K. B. Astroelectrochemistry: the role of redox reactions in cosmic dust chemistry. *Phys. Chem. Chem. Phys.* **12**, 3072–3079 (2010).
3. Bard, A. J. & Faulkner, L. R. *Electrochemical Methods: Fundamentals and Applications* 2nd edn, p.123 (Wiley, 2000).
4. Ghoroghchian, J. et al. Electrochemistry in the gas-phase—use of ultramicroelectrodes for the analysis of electroactive species in gas-mixtures. *Anal. Chem.* **58**, 2278–2282 (1986).
5. Vijh, A. K. Electrode-potentials and interface plasmons in the metal gaseous electrolyte (i.e., plasma) interphasic region. *Mater. Chem. Phys.* **14**, 47–56 (1986).
6. Vennekamp, M. & Janek, J. Plasma electrochemistry in radio frequency discharges - oxidation of silver in a chlorine plasma. *J. Electrochem. Soc.* **150**, C723–C729 (2003).
7. Ogumi, Z., Uchimoto, Y. & Takehara, Z. Electrochemistry using plasma. *Adv. Mater.* **7**, 323–325 (1995).
8. Hickling, A. & Ingram, M. D. Contact contact glow-discharge electrolysis. *Transactions of the Faraday. Society* **60**, 783–793 (1964).
9. Caruana, D. J. & McCormack, S. P. Electrochemistry in flames: a preliminary communication. *Electrochem. Commun.* **2**, 816–821 (2000).
10. Elahi, A., Fowowe, T. & Caruana, D. J. Dynamic electrochemistry in flame plasma electrolyte. *Angew. Chem. Int. Ed. Engl.* **51**, 6350–6355 (2012).
11. Elahi, A. & Caruana, D. J. Plasma electrochemistry: voltammetry in a flame plasma electrolyte. *Phys. Chem. Chem. Phys.* **15**, 1108–1114 (2013).
12. Frenklach, M., Wang, H. & Rabinowitz, M. J. Optimisation and analysis of large chemical kinetic mechanisms using the solution mapping method - Combustion of Methane. *Progress. Energy Combust. Sci.* **18**, 47–73 (1992).
13. Fowowe, T., Hadzifezovic, E., Hu, J., Foord, J. S. & Caruana, D. J. Plasma electrochemistry: development of a reference electrode material for high temperature plasma. *Adv. Mater.* **24**, 6305–6309 (2012).
14. Christensen, M. & Konnov, A. A. Laminar burning velocity of acetic acid plus air flames. *Combust. Flame* **170**, 12–29 (2016).
15. Gallois, N., Templier, J. & Derenne, S. Pyrolysis-gas chromatography-mass spectrometry of the 20 protein amino acids in the presence of TMAH. *J. Anal. Appl. Pyrolysis* **80**, 216–230 (2007).
16. Chiavari, G. & Galletti, G. C. Pyrolysis-gas chromatography/mass spectrometry of amino acids. *J. Anal. Appl. Pyrolysis* **24**, 123–137 (1992).
17. Rienstra-Kiracofe, J. C., Tschumper, G. S., Schaefer, H. F., Nandi, S. & Ellison, G. B. Atomic and molecular electron affinities: photoelectron experiments and theoretical computations. *Chem. Rev.* **102**, 231–282 (2002).
18. Sarathy, S. M., Osswald, P., Hansen, N. & Kohse-Hoinghaus, K. Alcohol combustion chemistry. *Progress. Energy Combust. Sci.* **44**, 40–102 (2014).
19. Aranda, V. et al. Experimental and kinetic modeling study of methanol ignition and oxidation at high pressure. *Int. J. Chem. Kinet.* **45**, 283–294 (2013).
20. Skreiberg, O., Kilpinen, P. & Glarborg, P. Ammonia chemistry below 1400 K under fuel-rich conditions in a flow reactor. *Combust. Flame* **136**, 501–518 (2004).
21. Mendiara, T. & Glarborg, P. Ammonia chemistry in oxy-fuel combustion of methane. *Combust. Flame* **156**, 1937–1949 (2009).
22. Ferrari, A. C. Raman spectroscopy of graphene and graphite: disorder, electron-phonon coupling, doping and nonadiabatic effects. *Solid State Commun.* **143**, 47–57 (2007).
23. Gao, Y. X. et al. Mechanistic study on the interfacial variation of carbon electrode under electrochemical oxidation. *J. Electroanal. Chem.* **783**, 90–99 (2016).
24. Gerischer, H. *Advances in Electrochemistry and Electrochemical Engineering*. Vol. 1 (ed. Delahay, D.) 139–232 (Interscience, New York, 1961).
25. Girault, H. H. *Analytical and Physical Electrochemistry* 1st edn, p.375 (EPFL Press, 2004).
26. Richmonds, C. et al. Electron-transfer reactions at the plasma-liquid interface. *J. Am. Chem. Soc.* **133**, 17582–17585 (2011).
27. King, I. R. & Calcote, H. F. Effect of probe size on ion concentration measurements in flames. *J. Chem. Phys.* **23**, 2203–2204 (1955).
28. Maclatchy, C. S. & Smith, H. C. L. The electron current to a langmuir probe in a flowing high-pressure plasma. *IEEE Trans. Plasma Sci.* **19**, 1254–1258 (1991).
29. Axford, S. D. T., Goodings, J. M. & Hayhurst, A. N. Mass-spectrometric sampling of ions from flames at atmospheric pressure: the effects of applied electric fields and the variation of electric potential in a flame. *Combust. Flame* **114**, 294–302 (1998).

Acknowledgements

The authors acknowledge the EPSRC (EP/H049398/1), for financial support. A.E. and M.C. wish to thank EPSRC for studentships. Our thanks go to Prof Stefan Howorka (UCL) for assistance with the manuscript preparation and Dr Jonathan Burns for help with preparation of Fig. 1. The EPSRC core capability for Chemistry research (EP/K03930X/1) grant for purchase of the Hiden HPR-60 MBMS Mass spectrometer. J. Stevenson for his technical expertise for building the electrode assembly and assembly for MS sampling.

Author contributions

The idea for this experiment was conceived by D.J.C. Method development was undertaken by D.J.C., A.E. and M.C., and the electrochemical data were collected by A.E. M.C. collected the Raman and MS data. D.J.C. wrote the paper and M.C. and A.E. contributed to the manuscript.

Additional information

Supplementary information accompanies this paper at <https://doi.org/10.1038/s42004-018-0046-7>.

Competing interests: The authors declare no competing interests.

Reprints and permission information is available online at <http://npg.nature.com/reprintsandpermissions/>

Publisher's note: Springer Nature remains neutral with regard to jurisdictional claims in published maps and institutional affiliations.



Open Access This article is licensed under a Creative Commons Attribution 4.0 International License, which permits use, sharing, adaptation, distribution and reproduction in any medium or format, as long as you give appropriate credit to the original author(s) and the source, provide a link to the Creative Commons license, and indicate if changes were made. The images or other third party material in this article are included in the article's Creative Commons license, unless indicated otherwise in a credit line to the material. If material is not included in the article's Creative Commons license and your intended use is not permitted by statutory regulation or exceeds the permitted use, you will need to obtain permission directly from the copyright holder. To view a copy of this license, visit <http://creativecommons.org/licenses/by/4.0/>.

© The Author(s) 2018